Analytical formulation of friction contact elements for frequency-domain analysis of nonlinear vibrations of structures with high-energy rubs

Article (Accepted Version)

ANALYTICAL FORMULATION OF FRICTION CONTACT ELEMENTS FOR FREQUENCY-DOMAIN ANALYSIS OF NONLINEAR VIBRATIONS OF STRUCTURES WITH HIGH-ENERGY RUBS

E.P. Petrov

University of Sussex, School of Engineering and Informatics,
Brighton BN1 9QT, United Kingdom, Email: y.petrov@sussex.ac.uk

ABSTRACT

In gas-turbine engines and other rotating machinery structures rubbing contact interactions can occur when the contacting components have large relative motion between components: such as in rotating bladed disc-casing rubbing contacts, rubbing in rotor bearing and labyrinth seals, etc. The analysis of vibrations of structures with rubbing contacts requires the development of a mathematical model and special friction contact elements that would allow for the prescribed relative motion of rubbing surfaces in addition to the motion due to vibrations of the contacting components.

In the proposed paper, the formulation of the friction contact elements is developed which includes the effects of the prescribed relative motion on the friction stick-slip transitions and, therefore, on the contact interaction forces. For a first time, the formulation is made for the frequency domain analysis of coupled rubbing and vibrational motion, using the multiharmonic representation of the vibration displacements. The formulation is made fully analytically to express the multiharmonic contact interaction forces and multiharmonic tangent stiffness matrix in an explicit analytical form allowing their calculation accurately and fast. The dependency of the friction and contact stiffness coefficients on the energy dissipated during high-energy rubbing contacts and, hence, on the corresponding increase of the contact interface temperature is included in the formulation.

The efficiency of the developed friction elements is demonstrated on a set of test cases including simple models and a large-scale realistic blade.

INTRODUCTION

Friction is one of the most important sources of nonlinear behaviour, damping and, in some cases, self-excitation of vibrations in gas-turbine and other machinery structures. The beginning of understanding and modelling of friction is usually attributed to works of G. Amontons in 17th century and then C.A. Coulomb in 18th century (see Coulomb's prize-winning paper in [1] or in later reprints of this paper). The Amontons-Coulomb friction model is still rather widely used in many studies, although a large number of new friction models has been developed to reflect some new experimental facts. There are good reviews of such models, developed mostly for the needs of mechatronics and servo-machines (e.g. see [2-4]).

In gas-turbine engines and many other machinery structures there are two major types of the friction contact interactions which need to be analysed: (i) the micro and macro slip friction interactions resulting from vibrations of a structure (such as friction at blade root joints, blade shroud contacts, underplatform and other friction damper devices, bolted joints, etc.) and (ii) friction contact interactions with or without vibrations accompanied by a rubbing motion which exceeds usually significantly the level of vibration amplitudes (blade-casing rubs, rubbing in bearing, seals, braking disks etc.)

The friction modelling in bladed disks for the first of the mentioned types started from using a slider friction model with the straight-line motion trajectory (see [5,6]) which were later generalised for two-dimensional motion ([7,8]) and finally for three-dimensional motion (see [9,10]). The fully analytical formulation of the friction damper model has been proposed for multiharmonic balance equations of motion in [11]. The modification allowing for the coupling between static and dynamic deformation components was suggested in [12]. A thorough review of friction modelling and numerical methods for analysis of gas-turbine structures is published recently in [13].

The second type of friction interaction is considered mostly

in papers on the analysis of rotor and whole engine dynamics (see e.g. a review in [14] and [15,16]) and in the analysis of blade tip – casing rubbing analysis (e.g. see [17]). Good descriptions of the friction contact modelling for rotor-casing and blade-casing rubs are given in [18,19]. The rubbing interaction between braking disks and pads represents another important example of this type of friction interaction. The energy resulting from friction interaction between a rotating brake disk and pads can produce self-excitation vibrations and, therefore, brake squeal in braking systems. The review of modelling brake squeal approaches can be found in [20]. The friction forces generate significant amount of heat energy, during gross rubbing, which can affect rotor vibration and the examples of analysis of the rotor dynamics allowing for the heat generation rubbing on the rotor dynamics are given in [21] and [22], where the rotor shaft bow due to friction-generated heat is included into coupled thermo-elastic equations.

In the papers considering the rubbing motion at the contacts, the effect of vibration of the rubbing components on the slip-stick transitions at the friction contact interface is usually ignored and assumed that the friction forces are fully governed by the sign of the velocity of gross rubbing motion used in the Amontons-Coulomb friction model. Yet, in many practical cases, a structure is subjected to periodic excitation and its vibrations can be significantly affected by the rubbing motion and vice versa. This effect can be noticed even when the amplitudes of vibrations are much smaller than the displacements of rubbing motion. Not displacement amplitudes but velocities of vibratory and rubbing motions determine the necessity of considering the coupling of both these motions in the friction modelling. Small but high frequency vibrations can produce velocities comparable to the velocities of large rubbing motion.

In the proposed paper, a friction model is developed which allows for the consistent description of the coupled effects of the prescribed rubbing motion and the vibration motion on the stick-slip transitions. The model is valid in the whole range of the rubbing motion velocities: from the case when the gross rubbing motion is absent to the case when the rubbing velocity is so large that the stick state does not occur and the permanent slip can only exist. The model includes the case of motion when, due to large vibrations along direction normal to the contact surfaces, contact-separation transitions occur.

The model is developed for the frequency-domain multiharmonic analysis of the nonlinear periodic vibrations. All matrices and vectors necessary for the Newton-Raphson iterative solution of the multiharmonic nonlinear equations of motion are derived in the analytical form, which provides the possibility of their accurate and fast solution. The most general case of the rubbing motion providing the periodic motion is considered: when the rubbing motion is represented as a sum of motion with a constant velocity and a periodic motion with a period common with the period of the excitation forces.

The friction element created here allows the calculation of: (i) forced response excited by external forces and (ii) the parametrically excited vibrations due to the periodic rubbing motion.

The effects of the heat generation at the contact interface on the friction contact parameters: friction coefficient and tangential and normal stiffness are also included in the formulation of the friction contact element. The calculation of the contact parameters corresponding to the vibration regime is based on an experimentally defined dependency of contact parameters on the contact temperature and the calculated correlation between the calculated dissipated power and the contact temperature. A nonlinear problem is formulated for the contact parameter calculation and an effective iterative solution procedure is proposed. The major capabilities of the developed friction model and the friction contact element are demonstrated on one degree of freedom (DOF) model and large-scale model of a realistic turbine blade.

FORMULATION OF THE NONLINEAR VIBRATION PROBLEM FOR STRUCTURES WITH RUBS

The equation of motion for the forced vibrations of a structure with nonlinear interactions at joints can be written in the form:

$$\boldsymbol{K}\boldsymbol{x}(t)+\boldsymbol{C}\dot{\boldsymbol{x}}(t)+\boldsymbol{M}\ddot{\boldsymbol{x}}(t)+\boldsymbol{f}(\boldsymbol{x}(t),\boldsymbol{u}(t))=\boldsymbol{p}(t) \qquad (1)$$

where $\boldsymbol{x}(t)$ is a vector of displacements for all degrees of freedom in the structure considered; $\boldsymbol{K}$, $\boldsymbol{C}$ and $\boldsymbol{M}$ are structural stiffness, damping and mass matrices of finite element (FE) model of a structure and $\boldsymbol{p}(t)$ is a vector of excitation forces; $\boldsymbol{p}(t)$ is a vector of periodic excitation forces; $\boldsymbol{f}(\boldsymbol{x}(t),\boldsymbol{u}(t))$ is a vector of nonlinear contact interface forces, and $\boldsymbol{u}(t)$ is a vector of a prescribed motion of all or some components of a structure analysed.

It is assumed that the prescribed motion, $\boldsymbol{u}(t)$, is known, for example, being determined from multibody dynamics equations, or defined by the kinematics of the structural components. In many cases the displacement described by this motion is much larger than the vibratory displacements, $\boldsymbol{x}(t)$, caused by the excitation forces, $\boldsymbol{p}(t)$. It should be noted that the prescribed motion, $\boldsymbol{u}(t)$, can excite the forced vibration in addition to the excitation forces, $\boldsymbol{p}(t)$.

The case of periodic excitation forces is considered, $\boldsymbol{p}(t)=\boldsymbol{p}\left(t+T_p\right)$, where T_p is the forces' period, and the periodic forced response is analysed. In order to ensure the periodicity of the forced response we have to impose a constraint on the prescribed motion variation over time. The most general case is considered here, when $\dot{\boldsymbol{u}}\left(t\right)=\dot{\boldsymbol{u}}\left(t+T_u\right)$ where T_u is the period of the prescribed motion velocities. Moreover, the ratio of the periods of the excitation force and the prescribed motion velocity should be a rational number, i.e.

$$T_p / T_u = j_1 / j_2 \qquad (2)$$

where j_1 and j_2 are integer numbers. Then the period of the forced response resulting from the action of these two sources of the excitation is:

$$T=\left(T_p / j_1\right) lcm\left(j_1, j_2\right) \qquad (3)$$

where $lcm(j_1, j_2)$ is the least common multiplier of j_1 and j_2.

The solution of periodic forced response of such a structure can be efficiently obtained with the multiharmonic balance method in conjunction with the Newton-Raphson method (see [11]). The efficiency and robustness of the solution process can be achieved by accurate and fast evaluation of the multiharmonic equation of motion and its extended Jacobian. To do this, we derive here analytical expressions for multiharmonic contact forces, stiffness matrix and other expressions for the friction contact elements with rubbing friction contacts.

FORCES AT THE RUBBING FRICTION INTERFACE

In order to derive the expressions for friction interface, we consider the relative motion of the contacting nodes of two surfaces where the tangential displacements are described by displacements $x_1(t)$ and $x_2(t)$, and the normal displacements are described by displacements, $y_1(t)$ and $y_2(t)$ (see Fig. 1). The prescribed rubbing motion along tangential direction, $u(t)$, is added to the vibrational motion of second contact surface to have its overall displacement in the global coordinate system: $x_2(t) - u(t)$.

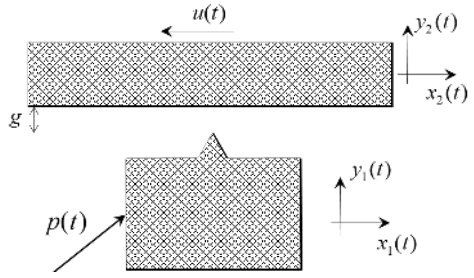

Fig. 1. Contact interface between two rubbing surfaces

The friction contact forces are dependent on the rubbing motion, $u(t)$, and on relative vibrational motion of the contacting surfaces:

$$x(t) = x_1(t) - x_2(t); \quad y(t) = y_1(t) - y_2(t) \tag{4}$$

Since the periodic vibrations are analysed, the relative vibrational motion can be expanded in a restricted Fourier series. Introducing here non-dimensional time $\tau = \omega t$, where $\omega = 2\pi / T$ is the principal vibration frequency, we obtain:

$$x(\tau) = \boldsymbol{H}_-^T(\tau)\boldsymbol{X}; \quad y(\tau) = \boldsymbol{H}_-^T(\tau)\boldsymbol{Y} \tag{5}$$

where $\boldsymbol{X} = \boldsymbol{X}_1 - \boldsymbol{X}_2$, and $\boldsymbol{Y} = \boldsymbol{Y}_1 - \boldsymbol{Y}_2$ are vectors of harmonic coefficients of relative vibrational motion in the tangential and normal directions and vector $\boldsymbol{H}_-$ takes the form:

$$\boldsymbol{H}_- = \{1, \cos m_1\tau, \sin m_1\tau, ..., \cos m_n\tau, \sin m_n\tau\}^T \tag{6}$$

where m_j $(j = 1..n)$ are the harmonic numbers included in the multiharmonic expansion of the forced response.

It was found that the most general form of the rubbing motion, which can provide the periodic vibration, can be represented as sum of motion with constant velocity, $\tilde{v}$, and the periodic motion with the period the motion defined in Eq.(3):

$$u(t) = \tilde{v}t + \boldsymbol{H}_-^T(\omega t)\boldsymbol{U} \tag{7}$$

or in the non-dimensional time:

$$u(\tau) = v\tau + \boldsymbol{H}_-^T(\tau)\boldsymbol{U} \tag{8}$$

where $v = \tilde{v}/\omega$ and $\boldsymbol{U}$ is the vector of harmonic coefficients of the periodic part of the rubbing motion. It should be noted that in many practical cases, this part is absent and only the motion with constant velocity can be considered. Moreover, the approach developed here can be applied for cases when the velocity v is varying over time, provided the rate of velocity variation is small enough to allow consideration of the vibrations as periodic – this is also quite common in practical applications.

Contact surface mechanical properties are characterised by a friction coefficient, μ, and stiffness coefficients along tangential direction, k_t and normal direction, k_n. The stiffness coefficients characterise elastic deformation of the asperities of the contacting rough surfaces in the tangential and normal directions respectively. Moreover, an initial gap between two contacting surfaces, g, can also be prescribed. The general case is considered here, when the gap value can be positive or negative. The later correspond to initial interferences, when the initial static pressure is applied at the contact interface.

Two components of the forces can occur during vibration: (i) normal and (ii) tangential forces. The time-domain expressions for these forces have common features with the expressions developed in [11], the major difference is the addition of the rubbing motion term in the expressions for the tangential force and allowing for the rubbing motion effects on the stick-slip transitions.

Normal contact interaction force

The motion along the normal direction, $y(\tau)$, determines whether the interacting surfaces are in contact or separated. The normal contact force is expressed as

$$f_y(\tau) = \begin{cases} k_n\left(y(\tau) - g\right) & \text{for contact} \\ 0 & \text{for separation} \end{cases} \tag{9}$$

Transitions from separation to contact and from contact to separation occur when normal displacement is equal to the gap value. The corresponding time instants are determined from the equation:

$$y(\tau) - g = 0 \tag{10}$$

The sign of the normal velocity, $\dot{y}(\tau)$, at these transitions determines the type of such a transition. When $\dot{y}(\tau) > 0$ at the transition time then this is a transition from separation to contact, otherwise it is a transition from contact to separation.

Tangential contact interaction force

The tangential contact force occurs only when the gap is closed and the contact surfaces come in contact, otherwise it is zero. In the expressions for the tangential force derived below, we assume that the surfaces are in contact. During contact, two different states of the friction contact interface are possible: slip or stick. In slip, the tangential force, f_x, is a dry friction force

and in the stick state, this force is due to elastic asperity deformations. Taking into account the influence of the variable normal force occurring during motion along normal direction and the rubbing motion defined by $u(\tau)$, expressions for non-linear interaction forces can be derived for the possible states in the following form:

$$f_x(\tau) = \begin{cases} f_x^0 + k_t(x(\tau) - x_0 + u(\tau) - u_0) & \text{for stick} \\ \xi \mu f_y(\tau) & \text{for slip} \end{cases} \quad (11)$$

where $x_0 = x(\tau_{stick})$, $u_0 = u(\tau_{stick})$ and $f_x^0 = f_x(\tau_{stick})$, are values of the relative tangential displacement, prescribed rubbing displacement and the tangential force at the beginning of the stick state, τ_{stick}, respectively; $\xi = \pm 1$ is a sign function of the tangential force at the time instant of slip state initiation, τ_{slip}.

For the considered case of rubbing friction contact, we generalise here the conditions of the stick-slip transition derived in [11]. The stick to slip transition occurs when the tangential interaction force of the stick state, $f_x(t)$, reaches this limiting value, $\mu f_y(t)$ i.e. when:

$$f_x^0 + k_t\left(x(\tau) - x_0 + u(\tau) - u_0\right) = \pm \mu k_n \left(y(\tau) - g\right) \quad (12)$$

Eq.(12) is solved with respect to time for both values of the sign for the limiting friction force. The lower value of τ gives the time of the stick-to-slip transition and the sign used in the equation gives the magnitude of the sign function, $\xi = \mathrm{sgn}(f_x(\tau_{slip}))$.

Equality of rates of stick and slip tangential force variation in time then allows us to write out an equation for slip-to-stick transition in the form:

$$\xi k_t\left(\dot{x}(\tau) + \dot{u}(\tau)\right) = \mu k_n \dot{y}(\tau) \quad (13)$$

To select from all possible solutions of Eq.(13) only those instants satisfying time instants when the stick state starts the following condition has to be checked:

$$\xi k_t\left(\ddot{x}(\tau) + \ddot{u}(\tau)\right) < \mu k_n \ddot{y}(\tau) \quad (14)$$

This condition ensures larger rate of increase for the limiting friction force (determined by the normal load) than the rate of increase of the friction force at the found time instant.

PERIODIC FRICTION STATE TRANSITION TIMES

Since periodic steady-state vibrations are analysed here, the periodic set of instants for state transitions has to be calculated in order to provide the periodic variation of non-linear interface forces.

Contact-separation transitions

The periodic set of contact-separation times is obtained simply by solving Eq.(10) over period of the vibrations. For the non-dimensional time all roots of this equation are calculated over period $[0, 2\pi]$ and intervals starting with $\dot{y}(\tau) > 0$ corresponds to the contact state.

Stick-slip transitions

Determination of stick-slip transitions is performed differently for two possible cases: (i) a case when there are contact-separation transitions and (ii) a case when the contact interface surfaces are in contact over the whole vibration period.

A case of the presence of contact-separation transitions. For this case, stick-slip transitions are determined for each contact interval independently. Firstly, the friction state is checked at the very beginning of the contact interval (i.e. at time τ_c) using the condition of the stick state existence – the absolute value of the tangential force increase rate should be smaller than the rate of the normal force increase:

$$\left|\dot{f}_x(\tau_c)\right| < \mu \dot{f}_y(\tau_c) \quad (15)$$

or substituting here the expressions for the tangential and normal forces this condition takes the form:

$$k_t\left|\dot{x}(\tau_c) + \dot{u}(\tau_c)\right| < \mu k_n \dot{y}(\tau_c) \quad (16)$$

If this condition is satisfied then at the start there is stick state. If instead of the inequality, we have equality in Eq.(16), then Eq.(14) allows the determination whether there is stick state at the starting contact time. In all other cases, the starting state is slip.

The initial values of displacements and tangential force used in Eq.(11) for the determination of the tangential force are calculated for the starting stick as follows:

$$x_0 = x(\tau_c); \quad u_0 = u(\tau_c); \quad f_x^0 = 0 \quad (17)$$

If the contact starts from slip then $\xi = \mathrm{sgn}(\dot{x}(\tau_c) + \dot{u}(\tau_c))$ and the expression for the tangential force in Eq.(11) is used for first slip state. When first state is known then all alternating stick and slip state transitions are found within the considered contact interval using Eqs.(12) and (13). It should be noted the possibility of only one state over the whole contact interval – this can be any of possible contact states: stick or slip.

A case of permanent contact. The case of permanent contact differs the most from the case considered in [11] where the rubbing was not considered. One of major differences is the possibility of full slip state (for large enough values of rubbing velocity, v) and the impossibility of the full stick state for all cases when $v \neq 0$.

To obtain the periodic set of state transition here we start from searching for the slip-to-stick transitions over period of vibration for the non-dimensional time, τ, $[0, 2\pi]$ using Eqs.(13) and (14) for two values of the sign $\xi = \pm 1$. If such transitions cannot be found then only slip exists over the whole vibration period and further search for state transitions stops. If the slip-to-stick transitions are found for both signs, then the stick time value, τ_0 is chosen from the slip-to-stick transitions found for the equation with sign ξ coinciding with the sign of the transitional velocity, v. This choice is necessary to ensure the correct calculation of slip states for cases of small vibration amplitudes, which for friction with $v = 0$ would provide the fully stuck state. For the case when $v \neq 0$ the sign of the slipping

velocity is defined by sign of v. For the starting stick state the following initial values are calculated:

$$x_0 = x(\tau_0); \quad u_0 = u(\tau_0); \quad f_x^0 = \xi \mu f_y(\tau_0) \qquad (18)$$

The value for ξ is used here which corresponds to the sign that is used in Eq. (13) for the found time τ_0. After this, all alternating stick and slip state transitions are searched within two vibration periods using Eqs.(12) and (13). For the periodic state transitions, the values obtained over the second period are taken to avoid some possible transitional effects.

Several scenarios of the forming of periodic variation of the friction force are illustrated in Fig. 2. The plots of the friction force obtained using the suggested above friction model for different values, v, for the rubbing velocity that is constant over time here (i.e. $\dot{u} = v$). The mono-harmonic vibrations for $x(\tau)$ and $y(\tau)$ are considered and the friction force is evaluated assuming that the normal pressure is the same for all considered cases. The non-dimensional time in this figure is the number of full cycles of vibrations. Small vibration amplitudes are considered here, but in all cases: with very small velocity values and with large velocity values the friction force reaches the limiting friction force value and the interface starts to slip. We can observe here that the rubbing velocity affects significantly the values of the friction forces when they start to vary periodically. The hysteresis loops plotted in Fig. 3 correspond to the periodic motions considered in Fig. 2. It is evident significant effect of the rubbing velocity on the hysteresis loops, even for the case of small amplitudes of vibration.

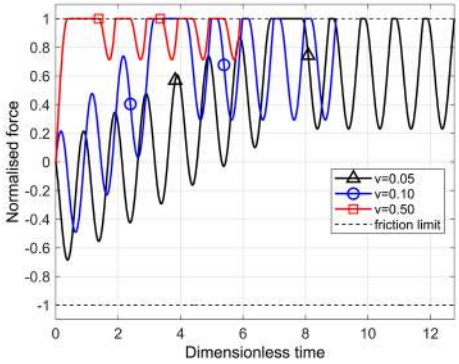

Fig. 2. Establishing of periodic variation of the friction force: a case of small vibration amplitudes

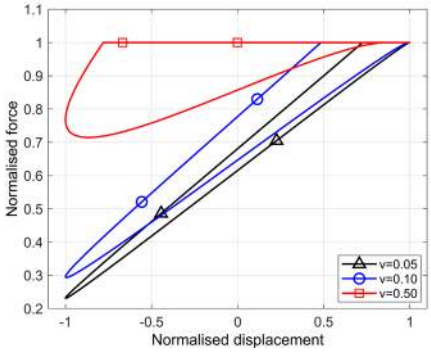

Fig. 3. Hysteresis loops for different transitional velocity: a case of small vibration amplitudes.

Other examples are shown for larger amplitudes in Fig. 4 and Fig. 5 where the cases of constant and variable pressures at the friction contact interface are considered.

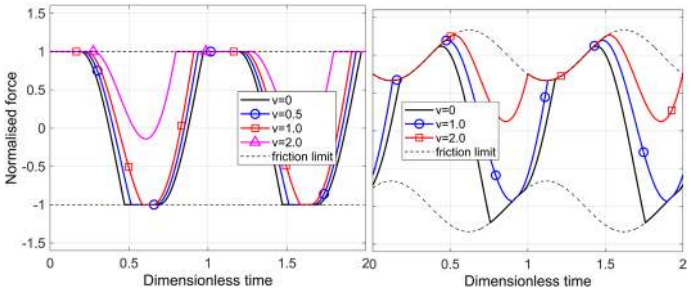

Fig. 4. The friction force: a case of large vibration amplitudes.

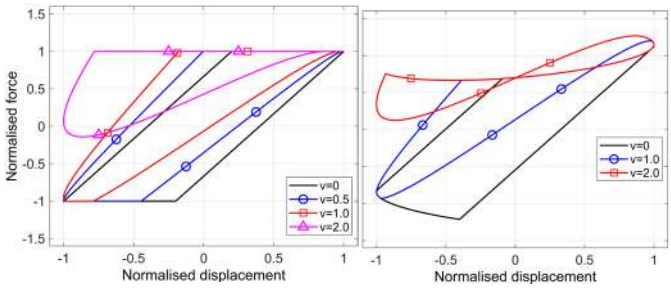

Fig. 5. Hysteresis loops: a case of large vibration amplitudes

One can see, again, the significant effect of the transitional velocity on the friction forces: the rubbing can cause the existence of only one (or in general case odd number) of stick state over period, which never happens in the conventional friction models when the rubbing motion is not allowed for. Further increase of the rubbing velocity can lead to the vibration without stick state at the contact interface.

MULTIHARMONIC CONTACT FORCES AND TANGENT STIFFNESS MATRIX

When the periodic set of friction state transition times is determined, then the vectors of multiharmonic expansion coefficients for tangential, $\boldsymbol{F}_x$, and normal, $\boldsymbol{F}_y$, forces can be calculated by integration of tangential and normal force expressions given by Eqs.(9) and (11) multiplied by the vector of harmonic functions, $\boldsymbol{H}_+$, over each interval of friction contact state:

$$\begin{Bmatrix} \boldsymbol{F}_x \\ \boldsymbol{F}_y \end{Bmatrix} = \begin{Bmatrix} \sum_{j=1}^{n_\tau} \boldsymbol{J}_x^{(j)} \\ \sum_{j=1}^{n_\tau^c} \boldsymbol{J}_y^{(j)} \end{Bmatrix} \qquad (19)$$

where n_τ and n_τ^c are the total numbers of stick- slip and contact-separation intervals accordingly. Introduced here integrals $\boldsymbol{J}_x^{(j)}$ and $\boldsymbol{J}_y^{(j)}$ over each interval of stick, slip and/or contact states have the form:

$$\boldsymbol{J}_x^{(j)} = \frac{1}{\pi}\int_{\tau_j}^{\tau_{j+1}} \boldsymbol{H}_+ f_x d\tau = \begin{cases} k_t \boldsymbol{W}_j^x \left(\boldsymbol{X}+\boldsymbol{U}\right) + k_t v \boldsymbol{w}_j^y + c_j \boldsymbol{w}_j^x & \text{stick} \\ \xi_j \mu k_n \left(-g\boldsymbol{w}_j^x + \boldsymbol{W}_j^x \boldsymbol{Y}\right) & \text{slip} \end{cases} \quad (20)$$

$$\boldsymbol{J}_y^{(j)} = \frac{1}{\pi}\int_{\tau_j^c}^{\tau_{j+1}^c} \boldsymbol{H}_+ f_x d\tau = \begin{cases} -k_n g \boldsymbol{w}_j^y + k_n \boldsymbol{W}_j^y \boldsymbol{Y} & \text{contact} \\ \boldsymbol{0} & \text{separation} \end{cases} \quad (21)$$

where $\boldsymbol{H}_+ = \left\{\frac{1}{2}, \cos m_1\tau, \sin m_1\tau, ..., \cos m_n\tau, \sin m_n\tau\right\}^T$; τ_j are instants of slip-stick transitions and τ_j^c are instants of contact-separation transitions. Other terms in these equations take the form:

$$\underset{(n\times n)}{\boldsymbol{W}_j^x} = \frac{1}{\pi}\int_{\tau_j}^{\tau_{j+1}} \boldsymbol{H}_+ \boldsymbol{H}_-^T d\tau\,; \quad \underset{(n\times n)}{\boldsymbol{W}_j^y} = \frac{1}{\pi}\int_{\tau_j^c}^{\tau_{j+1}^c} \boldsymbol{H}_+ \boldsymbol{H}_-^T d\tau \quad (22)$$

$$\underset{(n\times 1)}{\boldsymbol{w}_j^x} = \frac{1}{\pi}\int_{\tau_j}^{\tau_{j+1}} \boldsymbol{H}_+ d\tau\,; \quad \underset{(n\times 1)}{\boldsymbol{w}_j^y} = \frac{1}{\pi}\int_{\tau_j}^{\tau_{j+1}} \tau \boldsymbol{H}_+ d\tau\,; \; \underset{(n\times 1)}{\boldsymbol{w}_j^y} = \frac{1}{\pi}\int_{\tau_j^c}^{\tau_{j+1}^c} \boldsymbol{H}_+ d\tau \quad (23)$$

$$\begin{aligned} c_j &= f_x^0(\tau_j) - k_t\left[x(\tau_j)+u(\tau_j)\right] = \\ &= \xi_{j-1}\mu k_n\left(-g + y(\tau_j)\right) - k_t\left[x(\tau_j)+u(\tau_j)\right] \end{aligned} \quad (24)$$

Since the vectors used for transformation from time domain into frequency domain, $\boldsymbol{H}_+$, and for transformation back to time domain, $\boldsymbol{H}_-$, consist of sine and cosine functions of different orders, then the components of matrix $\boldsymbol{W}$ and vector $\boldsymbol{w}$ are simple integrals of sine and cosine functions and integrals of products of these functions. These integrals are calculated analytically, which provides an exact and very fast calculation for the vectors of Fourier expansion coefficients of the contact interface forces.

The tangent stiffness matrix of the friction interface element, $\boldsymbol{K}$, is determined as a matrix of derivatives of the multiharmonic vector of interface forces taken with respect to the multiharmonic coefficients of relative displacements. This matrix is obtained by differentiating Eq.(19) with respect to vectors $\boldsymbol{X}$ and $\boldsymbol{Y}$:

$$\boldsymbol{K} = \begin{bmatrix} \dfrac{\partial \boldsymbol{F}_x}{\partial \boldsymbol{X}} & \dfrac{\partial \boldsymbol{F}_x}{\partial \boldsymbol{Y}} \\ \boldsymbol{0} & \dfrac{\partial \boldsymbol{F}_y}{\partial \boldsymbol{Y}} \end{bmatrix} = \begin{bmatrix} \displaystyle\sum_{j=1}^{n_\tau} \frac{\partial \boldsymbol{J}_x^{(j)}}{\partial \boldsymbol{X}} & \displaystyle\sum_{j=1}^{n_\tau} \frac{\partial \boldsymbol{J}_x^{(j)}}{\partial \boldsymbol{Y}} \\ \boldsymbol{0} & \displaystyle\sum_{j=1}^{n_\tau^c} \frac{\partial \boldsymbol{J}_y^{(j)}}{\partial \boldsymbol{Y}} \end{bmatrix} \quad (25)$$

where:

$$\frac{\partial \boldsymbol{J}_x^{(j)}}{\partial \boldsymbol{X}} = \begin{cases} k_t \boldsymbol{W}_j^x + \boldsymbol{w}_j^x \dfrac{\partial c_j}{\partial \boldsymbol{X}}\,; & \text{stick} \\ \boldsymbol{0} & \end{cases} \quad \frac{\partial \boldsymbol{J}_x^{(j)}}{\partial \boldsymbol{Y}} = \begin{cases} \boldsymbol{w}_j^x \dfrac{\partial c_j}{\partial \boldsymbol{Y}} & \text{stick} \\ \xi\mu k_y \boldsymbol{W}_j^x & \text{slip} \end{cases} \quad (26)$$

$$\frac{\partial \boldsymbol{J}_y^{(j)}}{\partial \boldsymbol{Y}} = \begin{cases} k_n \boldsymbol{W}_j^y & \text{contact} \\ \boldsymbol{0} & \text{separation} \end{cases} \quad (27)$$

The derivatives of the constant term, c_j, of the tangential force with respect to $\boldsymbol{X}$ and $\boldsymbol{Y}$ used in Eqs.(26) are determined by differentiating Eq.(24), which gives the following expressions:

$$\frac{\partial c_j}{\partial \boldsymbol{X}} = -k_t \boldsymbol{H}_-^T(\tau_j) + \dot{c}_j \frac{\partial \tau_j}{\partial \boldsymbol{X}}\,; \quad \frac{\partial c_j}{\partial \boldsymbol{Y}} = -\xi\mu k_n \boldsymbol{H}_-^T(\tau_j) + \dot{c}_j \frac{\partial \tau_j}{\partial \boldsymbol{Y}} \quad (28)$$

$$\dot{c}_j = \xi_{j-1}\mu k_n \dot{y}(\tau_j) - k_t\left[\dot{x}(\tau_j) + \dot{u}(\tau_j)\right] \quad (29)$$

It should be noted the product $\dot{c}_j \partial\tau_j / \partial \boldsymbol{X}$ and $\dot{c}_j \partial\tau_j / \partial \boldsymbol{Y}$ are equal to zero for all stick times that follow to slip. This is owing to $\dot{c}_j = 0$ at these time instants by definition of times when slip to stick transitions occurs. For cases when the stick occurs at the time when separated surfaces come into contact, the time of the stick beginning coincides with the time of contact beginning. Because of that it is independent of $\boldsymbol{X}$, i.e.

$$\frac{\partial \tau_{stick}}{\partial \boldsymbol{X}} = \boldsymbol{0} \quad (30)$$

and derivatives with respect to vector $\boldsymbol{Y}$ are obtained by differentiation of the contact condition given by Eq.(10):

$$\frac{\partial \tau_{stick}}{\partial \boldsymbol{Y}} = -\frac{1}{\dot{y}(\tau_{stick})} \boldsymbol{H}_-^T(\tau_{stick}) \quad (31)$$

There are two special cases when the expressions for the vector and the stiffness matrix can be written without calculation of a set of stick-slip transitions. These cases are: (i) the case of full separation and (ii) the case when contact is permanent and stick does not occur.

For the full separation case the contact forces and tangent matrix are equal to zero, i.e.:

$$\boldsymbol{F}_x = \boldsymbol{F}_y = \boldsymbol{0} \quad \text{and} \quad \boldsymbol{K} = \boldsymbol{0} \quad (32)$$

For the case of permanent slip, the expressions for vector of the forces and tangent matrix take the form:

$$\begin{Bmatrix} \boldsymbol{F}_x \\ \boldsymbol{F}_y \end{Bmatrix} = \begin{Bmatrix} sign(v)\mu k_n\left(\boldsymbol{Y} - g\boldsymbol{e}_1\right) \\ k_n \boldsymbol{Y} \end{Bmatrix}; \quad \boldsymbol{K} = \begin{bmatrix} \boldsymbol{0} & \boldsymbol{0} \\ \boldsymbol{0} & k_n \boldsymbol{I} \end{bmatrix} \quad (33)$$

where $\boldsymbol{e}_1 = \{1, 0, ...0\}^T$ and $\boldsymbol{I}$ is the identity matrix.

SENSITIVITY OF CONTACT FORCES TO VIBRATION FREQUENCY

The important feature of the friction under rubbing motion is the frequency dependency of the friction contact forces on the vibration frequency. This contrasts to the conventional perception that the dry friction is generally frequency-independent. The frequency dependency occurs for all cases when the linear component of the rubbing velocity is different from zero, i.e. $v \neq 0$, and when this velocity is small enough to allow slip-stick transitions. These conditions are satisfied for many practical cases of friction contacts with rubs. Therefore, to perform the solution continuation, when the excitation frequency is the tracing parameter, it is necessary to calculate not only the multiharmonic contact forces and the tangent matrix, as it is shown in the preceding section, but also the sensitivity of the contact forces to the principal vibration frequency, ω. The expression for these sensitivities can be also obtained analytically:

$$\frac{\partial}{\partial\omega}\begin{Bmatrix} \boldsymbol{F}_x \\ \boldsymbol{F}_y \end{Bmatrix} = \frac{\partial}{\partial\omega}\begin{Bmatrix} \displaystyle\sum_{j=1}^{n_\tau} \boldsymbol{J}_x^{(j)} \\ \displaystyle\sum_{j=1}^{n_\tau^c} \boldsymbol{J}_y^{(j)} \end{Bmatrix} = \begin{Bmatrix} \displaystyle\sum_{j=1}^{n_\tau} \frac{\partial}{\partial\omega} \boldsymbol{J}_x^{(j)} \\ \boldsymbol{0} \end{Bmatrix} \quad (34)$$

where

$$\frac{\partial \boldsymbol{J}_x^{(j)}}{\partial \omega} = \begin{cases} \left(k_t \dfrac{\partial v}{\partial \omega}\right) \boldsymbol{w}_j^v + \boldsymbol{w}_j^x \dfrac{\partial c_j}{\partial \omega} & \text{stick} \\ \boldsymbol{0} & \text{slip} \end{cases} \quad (35)$$

and $$\partial v / \partial \omega = -v / \omega; \quad \partial c_j / \partial \omega = k_t v \tau_j / \omega \quad (36)$$

MODELLING OF RUBBING ENERGY DISSIPATION EFFECTS ON CONTACT INTERFACE PARAMETERS

The friction contact interactions dissipate the energy of vibration and the energy of prescribing rubbing motion, $u(\tau)$, by transferring them into the thermal energy and into the generation of debris due to wear of the microasperities at the rough contact surfaces. When the dissipation energy is high, as it usually happens under high-energy rubs, the generated thermal energy is high enough to increase significantly the temperature at contact interfaces. It is experimentally confirmed (see, e.g. [23]) that the friction coefficient and other parameters of contact interfaces are dependent on the temperature, i.e.:

$$\mu = \mu\left(T^o\right); \; k_t = k_t\left(T^o\right); \; k_n = k_n\left(T^o\right) \quad (37)$$

where T^o is the temperature at the contact interface. The contact interface temperature is determined by the thermal conditions at which the structure operates, by the conductivity characteristics and by the amount of energy generated at contact interfaces due to friction forces. Hence, the temperature at a contact interface can be represented as a sum of background temperature, T_0^o – not related to the energy dissipated at contact interface and the temperature increase caused by the frictional rubs, T_r^o. The latter is dependent on the power of the energy dissipation at the contact interface, $\dot{E}$:

$$T^o = T_0^o + T_r^o\left(\dot{E}\right) \quad (38)$$

To determine the dissipated power, $\dot{E}$, firstly we obtain the expression for the energy dissipated over a period of vibrations, E:

$$\begin{aligned} E &= \int_0^{2\pi} f_x(\tau)\left[\dot{x}(\tau) + \dot{u}(\tau)\right] d\tau = \\ &= \int_0^{2\pi} \boldsymbol{F}_x^T \boldsymbol{H}_-(\tau)\left[v + \dot{\boldsymbol{H}}_-^T(\tau)\left(\boldsymbol{X} + \boldsymbol{U}\right)\right] d\tau = \\ &= 2\pi v \boldsymbol{e}_1^T \boldsymbol{F}_x + \pi\left(\boldsymbol{L}\left(\boldsymbol{X} + \boldsymbol{U}\right)\right)^T \boldsymbol{F}_x \end{aligned} \quad (39)$$

where

$$\boldsymbol{e}_1 = \{1, 0, ..., 0\}^T; \quad \boldsymbol{L} = diag\left(0, m_1 \begin{bmatrix} 0 & 1 \\ -1 & 0 \end{bmatrix}, ..., m_n \begin{bmatrix} 0 & 1 \\ -1 & 0 \end{bmatrix}\right) \quad (40)$$

Then, owing to small vibration period comparing to the time scale in which the temperature variation is considered, the dissipated power can be obtained by equalising the dissipation power to its value averaged over the period of vibration:

$$\dot{E} = \frac{\partial E}{\partial t} \simeq \frac{\omega}{2\pi} E = \omega\left[v \boldsymbol{e}_1^T \boldsymbol{F}_x\left(\boldsymbol{b}\right) + 0.5\left(\boldsymbol{L}\left(\boldsymbol{X} + \boldsymbol{U}\right)\right)^T \boldsymbol{F}_x\left(\boldsymbol{b}\right)\right] \quad (41)$$

The vector of multiharmonic contact forces, $\boldsymbol{F}_x\left(\boldsymbol{b}\right)$, is calculated as explained in previous sections. It is dependent on all contact interface parameters, combined here in a vector: $\boldsymbol{b} = \{\mu, k_t, k_n\}^T$

We can notice that Eq.(37) together with Eqs.(38) and (41) represents a nonlinear system of equations with respect to values of the contact interface parameters μ, k_t, and k_n:

$$\boldsymbol{R} = \begin{Bmatrix} \mu - \mu\left(T_0^o + T_r^o\left(\dot{E}\right)\right) \\ k_t - k_t\left(T_0^o + T_r^o\left(\dot{E}\right)\right) \\ k_n - k_n\left(T_0^o + T_r^o\left(\dot{E}\right)\right) \end{Bmatrix} = \boldsymbol{b} - \boldsymbol{b}\left(T_0^o + T_r^o\left(\dot{E}\left(\boldsymbol{b}\right)\right)\right) = \boldsymbol{0} \quad (42)$$

The solution of this equation is performed by Newton-Raphson iterative method:

$$\frac{\partial \boldsymbol{R}\left(\boldsymbol{b}_i\right)}{\partial \boldsymbol{b}}\left(\boldsymbol{b}_{i+1} - \boldsymbol{b}_i\right) = -\boldsymbol{R}\left(\boldsymbol{b}_i\right) \quad (43)$$

where i is the iteration number. The iterative solution process is performed for the fixed values of $\boldsymbol{X}$ and $\boldsymbol{Y}$ at each iteration the contact forces, $\boldsymbol{F}_x$ and the dissipation power $\dot{E}\left(\boldsymbol{b}, \boldsymbol{X}, \boldsymbol{F}_x\right)$ are calculated. For the starting point the values of contact interface parameters at the background temperature, T_0^o, can be used: $\boldsymbol{b}_0 = \boldsymbol{b}\left(T_0^o\right)$. The iterative solution of Eq.(43) can be performed for each friction contact element independently. So, the contact parameters are determined at the contact element level: to obtain the friction contact interface parameters corresponding to any given relative displacements $\boldsymbol{X}$ and $\boldsymbol{Y}$. When the friction interface parameters are found, the multiharmonic contact forces $\boldsymbol{F}_x$ and $\boldsymbol{F}_y$, the tangential stiffness matrix, $\boldsymbol{K}$, and $\partial \boldsymbol{F}_x / \partial \omega$ corresponding to found parameter values are calculated and they are used in forming the frequency-domain equations of motion for a structure analysed. In some cases the dependency of the temperature on the energy generated by all friction elements needs to be considered. In this case, the temperature of contact friction elements at a contact surface is coupled by the thermo-conductivity coefficients for a considered surface and the iterative determination of the contact parameters is performed for all contact elements located at this surface simultaneously.

Therefore, the harmonic coefficients of relative displacements, $\boldsymbol{X}$ and $\boldsymbol{Y}$ are considered as independent of the values of contact interface parameters when Eq.(43) is solved and only friction forces are treated as functions of the contact interface parameters. The iterations given by Eq.(43) are performed till the required accuracy in the parameter determination is achieved, which is controlled by the convergence condition: $\left\| \left(\boldsymbol{b}_{i+1} - \boldsymbol{b}_i\right) / \boldsymbol{b}_{i+1} \right\| < \varepsilon$ where the ε is a chosen small number used to control the relative accuracy of the contact parameters. When the solution of this equation is found, the contact force vector is obtained and the tangent stiffness matrix are evaluated for the found set of contact parameters corresponding to found thermal equilibrium allowing for the friction-generated heat.

At each iteration the residual vector $\boldsymbol{R}(\boldsymbol{b}_i)$ and the Jacobian, $\partial \boldsymbol{R}(\boldsymbol{b}_i)/\partial \boldsymbol{b}$ of Eq. (43) are calculated. The expressions for the Jacobian of Eq.(43) are derived analytically too. The general expression for the Jacobian takes the form:

$$\frac{\partial \boldsymbol{R}}{\partial \boldsymbol{b}} = \boldsymbol{I} - \frac{\partial \boldsymbol{b}}{\partial T^o}\frac{\partial T^o}{\partial \dot{E}}\frac{\partial \dot{E}}{\partial \boldsymbol{b}} \tag{44}$$

The derivatives, included in this equation, of the energy dissipation power with respect to contact parameters can be obtained by differentiating Eq.(41):

$$\frac{\partial}{\partial \gamma}\dot{E} = \omega\left[v\boldsymbol{e}_1^T \frac{\partial \boldsymbol{F}_x}{\partial \gamma} + 0.5\frac{\partial \boldsymbol{F}_x^T}{\partial \gamma}\boldsymbol{L}(\boldsymbol{X}+\boldsymbol{U})\right];\quad \gamma = \mu, k_t, k_n \tag{45}$$

The evaluation of these derivatives requires the calculation of sensitivity of the multiharmonic tangential contact force vector, $\boldsymbol{F}_x$, with respect to the contact parameters. The expressions for these sensitivities can be also derived analytically:

$$\frac{\partial}{\partial \gamma}\boldsymbol{F}_x = \sum_{j=1}^{n_c}\frac{\partial \boldsymbol{J}_x^{(j)}}{\partial \gamma};\quad \gamma = \mu, k_t, k_n \tag{46}$$

where the summands on the right side of Eq.(46) are obtained by differentiating Eq.(20) with respect to contact parameters. As a result, we obtain:

$$\frac{\partial \boldsymbol{J}_x^{(j)}}{\partial \mu} = \begin{cases} \dfrac{\partial c_j}{\partial \mu}\boldsymbol{w}_j & \text{stick} \\ \xi_j k_n\left(-g\boldsymbol{w}_j^x + \boldsymbol{W}_j^x \boldsymbol{Y}\right) & \text{slip} \end{cases} \tag{47}$$

$$\frac{\partial \boldsymbol{J}_x^{(j)}}{\partial k_t} = \begin{cases} \boldsymbol{W}_j^x(\boldsymbol{X}+\boldsymbol{U}) + v\boldsymbol{w}_j^v + \dfrac{\partial c_j}{\partial k_t}\boldsymbol{w}_j^x & \text{stick} \\ \boldsymbol{0} & \text{slip} \end{cases} \tag{48}$$

$$\frac{\partial \boldsymbol{J}_x^{(j)}}{\partial k_n} = \begin{cases} \dfrac{\partial c_j}{\partial \mu}\boldsymbol{w}_j & \text{stick} \\ \xi_j \mu\left(-g\boldsymbol{w}_j^x + \boldsymbol{W}_j^x \boldsymbol{Y}\right) & \text{slip} \end{cases} \tag{49}$$

where $\partial c / \partial \mu$ is determined by differentiating Eq.(24)

$$\frac{\partial c_j}{\partial \mu} = \xi k_n\left(-g + y(\tau_j)\right) + \dot{c}_j\frac{\partial \tau_j}{\partial \mu} = \xi k_n\left(-g + y(\tau_j)\right) \tag{50}$$

$$\frac{\partial c_j}{\partial k_t} = -\left[x(\tau_j) + u(\tau_j)\right] + \dot{c}_j\frac{\partial \tau_j}{\partial k_t} = -x(\tau_j) - u(\tau_j) \tag{51}$$

$$\frac{\partial c_j}{\partial k_n} = \xi\mu\left(-g + y(\tau_j)\right) + \dot{c}_j\frac{\partial \tau_j}{\partial k_n} = \xi\mu\left(-g + y(\tau_j)\right) \tag{52}$$

Here the fact that the product $\dot{c}_j\,\partial\tau_j/\partial\mu$ and $\dot{c}_j\,\partial\tau_j/\partial k_t$ are equal to zero for all stick starting time instants is taken into account. This is due to $\dot{c}_j = 0$ at these time instants by definition of times when slip to stick transitions occur. For special cases when the stick state after separated surfaces come into contact then another multiplier included in this product is equal to zero: $\partial\tau_j/\partial\mu = \partial\tau_j/\partial k_t = \partial\tau_j/\partial k_n = 0$, since these time instants are defined only by normal displacement variation and are not dependent on the contact parameters.

NUMERICAL EXAMPLES

The capabilities of the new friction contact interface model developed here to include large rubbing motion in the analysis of nonlinear vibrations of structures with contact interfaces has been explored on a number of simple systems and on realistic gas-turbine structures. In this paper the examples of application of this model to the analysis of two structures are shown: (i) a single-degree-of-freedom (SDOF) oscillator and (ii) a realistic blade.

A single degree of freedom oscillator

An SDOF oscillator was considered in order to explore the major properties of the new friction element. The equation of motion of the oscillator has the following form:

$$m\ddot{x} + c\dot{x} + kx + f(x + u(t), \dot{x} + \dot{u}(t)) = p\sin\omega t \tag{53}$$

where $m = 1$; $c = 0.4$; $k = 40$; $p = 100$ and $f = f_x$ is the friction force. The fiction force is calculated assuming that the tangential direction of the contact surface coincides with the direction of oscillator motion and the normal load is constant $f_y = k_n g = 800$. The friction coefficient is not affected by the dissipation energy here: $\mu = 0.3$ and the tangential contact interface stiffness is $k_t = 100$. All parameters of the model can be provided in any consistent system of units, such as [kg,m,sec,N] or [ton,mm,sec,N]. The frequency in the following figures is provided in rad/sec. In the multiharmonic nonlinear forced response calculations, first 11 harmonics are used: from 0 to 10.

Constant rubbing velocity cases. Firstly, the cases of the transitional rubbing motion with constant velocity are considered: $u(t) = vt$. The maximum dynamic amplitude and the static, zero component of the forced response are shown in Fig. 6 and Fig. 7 for different values of the rubbing velocity: from 0 to 250. The forced response of this system without the friction damper is also shown in these figures for comparison.

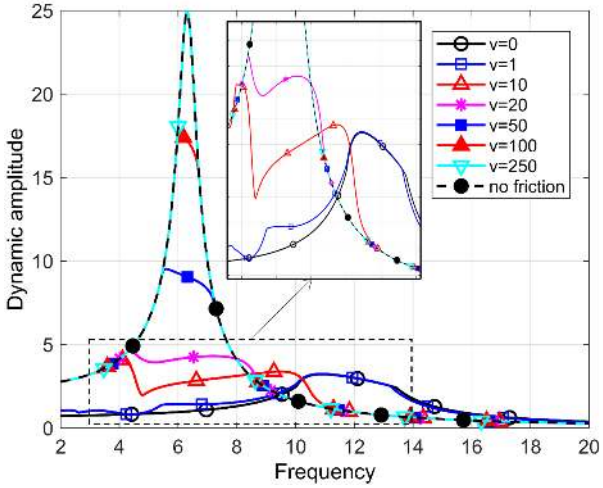

Fig. 6. Vibration amplitude for different rubbing velocity values: the SDOF oscillator

For large rubbing velocity $v = 250$ the stick state does not occur over the whole frequency range for this system and the dynamic forced response amplitude (calculated by the subtraction of zero harmonic component from the response) is identical to the amplitude of the system without damper. The maximum displacement value differs by the value of static displacement, which equal to $\mu N_0 / k = 6$ for a case of fully slipping interface. Observing the variation of the zero harmonic value over the frequency range in Fig. 7, we can see how the static equilibrium point varies with the variation of frequency.

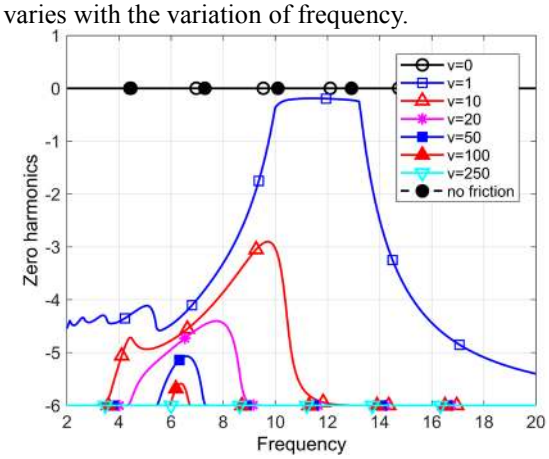

Fig. 7. Zero harmonic of the calculated forced response for different rubbing velocity values: the SDOF oscillator

For $v = 0$ and for the system without friction, zero harmonic component is equal to zero over the whole analysed frequency range. For $v = 1$ the zero harmonic is close to zero at the resonance peak while for the other values zero harmonic component is significant over the whole frequency range and takes values close to 6 for frequency ranges where these amplitude are smaller. Hence, for small rubbing velocity $v = 1$ the maximum displacement and the dynamic amplitude are close, in the vicinity of the resonance peak, to those of the system without rubbing, $v = 0$. This is because, for large vibration amplitudes, the vibratory motion is dominant in the stick-slip transitions at the contact interface. For out-of-resonance frequency ranges, where the vibration amplitudes are small, the large static component is observed, although the dynamic amplitude value is similar to the case of no rubbing. The plots corresponding to the values of rubbing velocity from 10 to 100 show a gradual change of the resonance frequency to the frequency of system without damper: 6.32 rad/s. It is evident also that the shape of resonance peaks differ significantly from those that are observed for a system without rubbing when such transition is achieved by reduction of the normal load (see for comparison results shown in [11]).

The results of calculations obtained by the multiharmonic balance methods are usually affected by the total number of harmonics used in the multiharmonic representation of the displacement and by the selection of these harmonic numbers. The extensive analysis of such effects on the analysis of simple and complex systems with rubbing has been performed. The analysis shows two significant distinctions of the analysis with rubbing from the analysis of structures with friction without rubbing: (i) necessity of using zero harmonic and (ii) importance of keeping even harmonics in the multiharmonic representation of displacements. As an example, in Fig. 8 the dynamic forced response of the considered above SDOF system is shown for a case of rubbing velocity $v = 10$. The results of three calculations are shown here when all (odd and even) harmonics are used: (i) from 0 to 3; (ii) from 0 to 7 and (iii) from 0 to 10. The case of calculation when zero and odd harmonic from 0 to 10 are also plotted. One can see that the curve corresponding to the case (ii) is fully hidden since it coincides with the curve (iii) and curve (i) is distinguishable only in a narrow frequency range close to the first resonance peak (in vicinity of frequency value 4 rad/s). The dynamic forced response curve obtained with only zero and odd harmonics used differs significantly over the large frequency range including both resonance peaks.

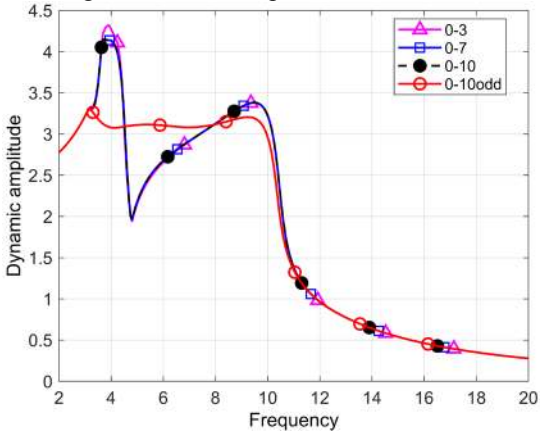

Fig. 8. Effect of harmonic numbers on vibration amplitude: the SDOF oscillator, $v = 10$

Oscillatory rubbing motion cases. In addition to the constant velocity the rubbing motion can have also periodically varied components and the effects of these components have been explored. The examples of the forced response obtained for a case when $u = vt + 2\cos\omega t$ for different values of v is shown in Fig. 9 and Fig. 10. We can notice the change of the resonance peak shapes comparing them with Fig. 6 and the occurrence of multiple resonance peaks in the low frequency range.

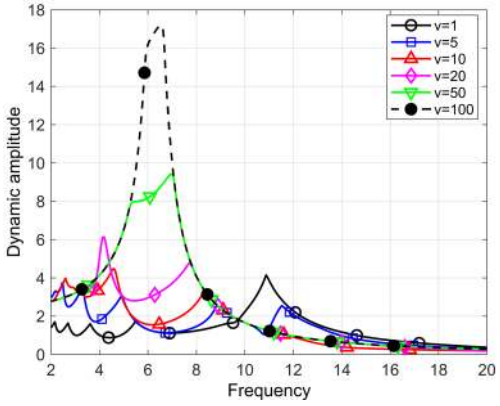

Fig. 9. Vibration amplitude for the SDOF oscillator with rubbing motion: $u = vt + 2\cos\omega t$

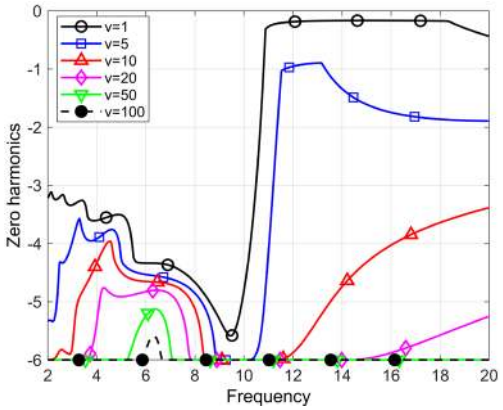

Fig. 10. Zero harmonic of the forced response for the SDOF oscillator with rubbing motion: $u = vt + 2\cos\omega t$

Parametric excitation by rubbing oscillatory motion. The rubbing periodic motion can cause the parametric excitation of vibration. An example the forced response excited by only the harmonic rubbing motion of the damper is shown in Fig. 11 for different amplitudes, a, of the rubbing motion $u = a\cos\omega t$. In all cases, the external excitation force is assumed zero: $p = 0$ and the excitation of the vibration occurs due to the rubbing motion at frictional contact interface. The resonance peaks differ in shape from the resonance peaks of the system damped by friction in the absence of rubbing, the resonance frequency decreases monotonically and the resonance amplitude decreases. The zero component of the forced response excited by the rubbing motion has zero value for all frequencies and, hence, is not plotted here.

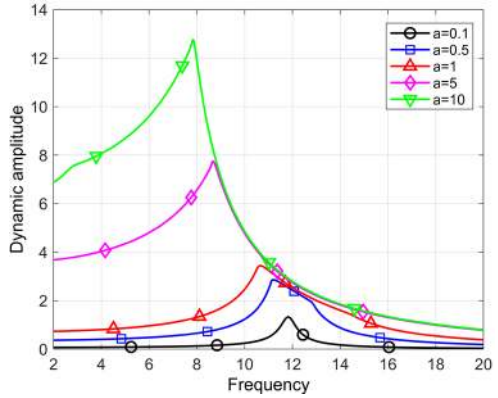

Fig. 11. Vibration amplitude for the SDOF oscillator with rubbing motion: $u = a\cos\omega t$ **in the absence of external force**

A turbine blade

For an example of the analysis of the rubbing motion on the vibration of large models of structures with friction contact interfaces a turbine blade finite element (FE) model shown in Fig. 12 is considered. The FE model comprises 101,200 DOFs. The blade is fixed at the blade root contact surfaces, 8 friction contact element are uniformly distributed over the surface at the blade shroud surface marked in green in Fig. 12.

The direction of the rubbing motion is indicated in this figure by the arrow and the rubbing motion with constant velocity is considered, i.e. $u = vt$. The casing is not included in the model and it is assumed that the friction contact elements rub against a rigid surface. The excitation of the vibration is performed by harmonic forces distributed over the finite element nodes of the concave blade surface. The frequency range including first blade resonance frequency is considered. For the analysis of nonlinear vibration of the blade, the high-accuracy reduction method developed in [24] is used. The forced response function (FRF) matrices are generated for the nodes where the friction contact element are applied. The FRF matrices are generated with the use of modal characteristics of a structure without contacts. The background frequency-independent modal damping factors are assumed for all 128 modes included in the reduced blade model equal to 0.001 (see [24] for the details of the model reduction method). The analysis of effects of number of harmonics included in the analysis has been performed and it was found that first 6 harmonics: from 0 to 5 provide sufficiently accurate solutions over the whole frequency range and for parameters analysed, therefore, these harmonics are used to obtain all results reported below.

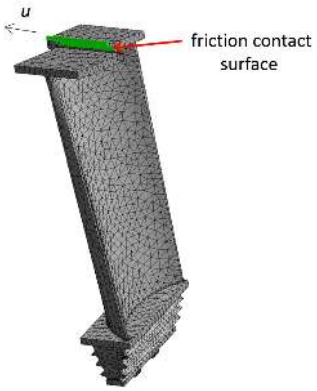

Fig. 12. Finite element model of the analysed blade

Two types of the analysis allowing for the rubbing effects have been performed: (i) the analysis when all friction contact interface parameter are considered constant irrelevantly of the dissipation energy and (ii) when the temperature increase effects on the friction coefficient values due to energy dissipation at contact interface are included in the analysis.

For the second type, the dependency of the friction coefficient on the temperature is used that is obtained from the experimental measurements reported in [23]. The cubic spline approximation of this dependency is performed using the table of experimental values. The spline approximation allows calculation not only the friction coefficient value for a given temperature but also its derivative with respect to the temperature, which is necessary for the evaluation of the matrix in Eq.(44). The correlation between the dissipated power at contact interface and its temperature is obtained by the solution of the linear steady-state conductivity problem with heat sources applied at the friction contact element locations. For this calculation, the blade finite element model shown in Fig. 12 is used with allowing for the convection heat transfer over the blade surfaces.

Analysis with constant values of friction interface parameters. At first, to obtain a reference case for the illustration of the rubbing effects, the forced response was calculated without the rubbing motion and assuming constant friction coefficient. The amplitudes of vibration obtained for different levels of the normal load, N_0, applied to the blade friction contact surface are shown Fig. 13 together with two limiting cases: (i) a blade without friction contacts and (ii) a blade with fully stuck contact elements. The normalised dissipation power is plotted for these cases in Fig. 14.

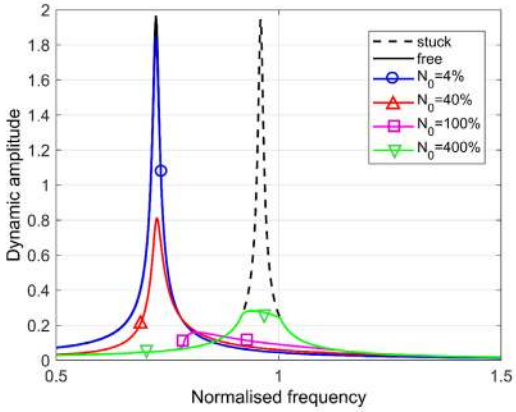

Fig. 13. Forced response amplitude for a blade without rubs

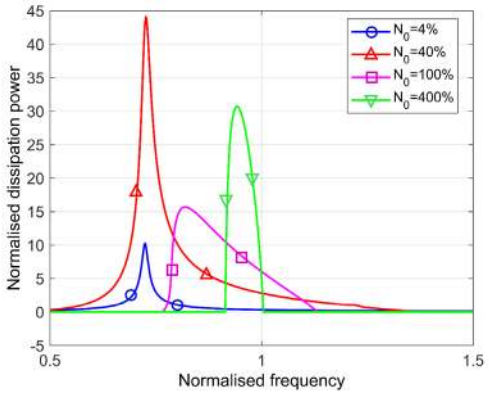

Fig. 14. Dissipation power for a blade without rubs

It should be noticed here that, although the dissipated energy is correlated in most cases with the reduction of the resonance vibration amplitude, for the case of friction damping the energy dissipation is only one of two mechanisms of such reduction: the second mechanism is the variation of the stiffness properties over vibration period. Because of this, we can observe that the maximum amplitude reduction is achieved for normal load of 100% while the maximum dissipated energy is observed here for the normal load 40%. More detailed discussion on these mechanisms can be found in [25].

The effect of the rubbing velocity on the dynamic forced response amplitude is shown for different levels of the normal load and the rubbing velocity in Fig. 15, Fig. 16 and Fig. 17. It is evident that for all levels of the normal loading the rubbing with large enough velocity (in our case $v = 10^4$) suppresses the damping effects of the friction contact on the vibrational amplitude and it becomes equal to the amplitude of the structure without friction. The rubbing motion affects significantly the resonance frequency values and the resonance amplitude. It is important to notice also the large effect of the rubbing motion on the out-of-resonance vibration amplitudes: the level of such vibrations can be changed due to rubbing by factor 2.5. The realistic values of rubbing velocity start from 5000 and higher for the case considered here.

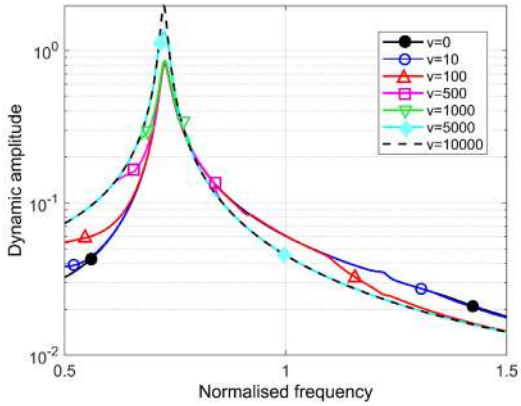

Fig. 15. Vibration amplitude for a blade with: $N_0 = 40\%$

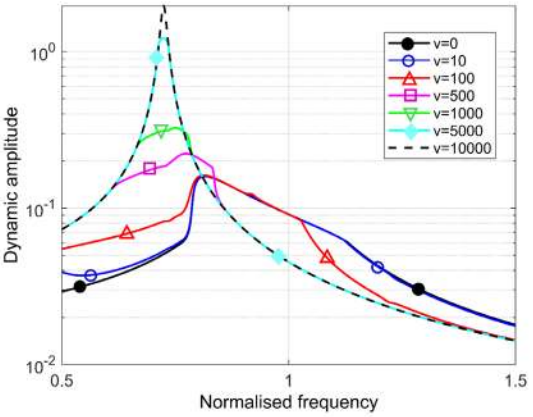

Fig. 16. Vibration amplitude for a blade with: $N_0 = 100\%$

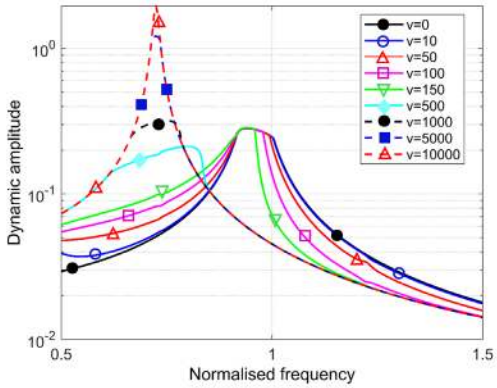

Fig. 17. Vibration amplitude for a blade with: $N_0 = 400\%$

Analysis considering the effects of the dissipation energy on friction coefficient. The examples of the analysis of blade vibration when the effects of friction-generated

dissipation energy on the friction coefficient through the contact temperature increase are shown in the following figures. A case of normal load $N_o = 20\%$ is considered here and the calculated forced response is shown in Fig. 18 (where the dynamic amplitudes are plotted), in Fig. 19 (where zero harmonic of the forced response is plotted) and in Fig. 20 (where the dissipated power is displayed).

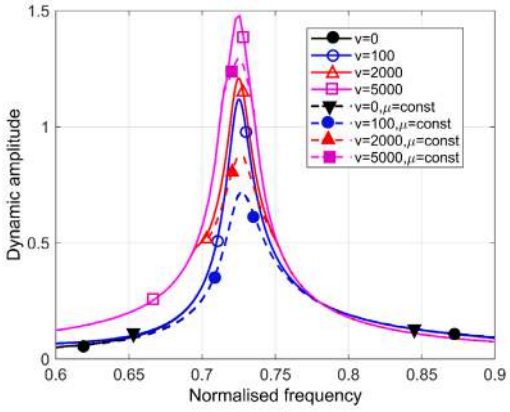

Fig. 18. Vibration amplitude for a blade with allowing for effects of dissipation energy on the friction coefficient

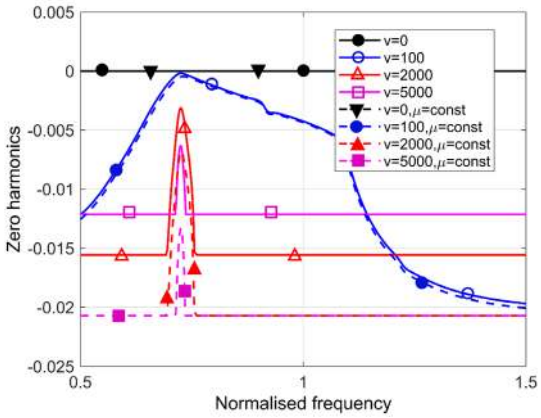

Fig. 19. Zero harmonic of the forced response for a blade with the friction coefficient affected by dissipation energy

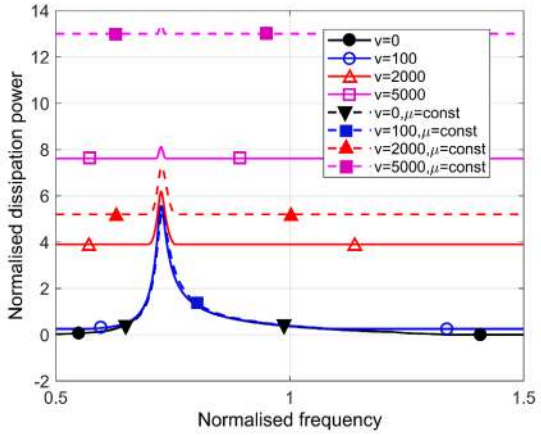

Fig. 20. Dissipated power dependency on the vibration frequency for the blade with rubs

The results are shown here for two friction modelling cases: (i) when the friction coefficients corresponding to the ambient temperature is used in the calculations and (ii) when the effect of dissipation energy on the friction coefficient is included in the model as it is described in the method developed in this paper.

We can see that the resonance amplitudes are significantly higher when we take into account the effect of the dissipation energy on the friction coefficient: which is due to the significant reduction of its value due to temperature increase because of energy dissipation. Such increase is larger for smaller values of the rubbing velocity: from 0 to 2000, while for $v = 5000$ this effect is smaller. It is important to notice the large change in the zero component of the vibration – the component defining the equilibrium around which the vibrations are performed. The effect of the dissipation energy is significant only for larger rubbing velocity values (in the considered cases they are 2000 and 5000). The dissipated power plots in Fig. 20 show that for large rubbing velocity the increase of the dissipation power at resonance peaks is rather small compared with the case of no rubbing ($v = 0$) or rubbing with small velocity ($v = 100$) when the vibration is the major source of the dissipation power. Allowing for the dependency of the friction coefficient on the temperature increase due to the dissipation can reduce by 50% the dissipation energy, especially for out-of-resonance frequencies.

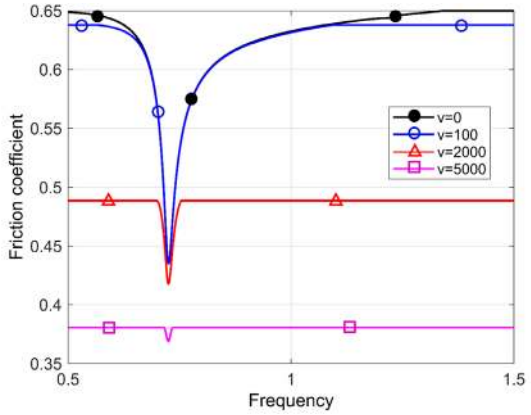

Fig. 21. Friction coefficient dependency on the vibration frequency due to effects of the dissipation energy

The change of the friction coefficient with the frequency variation is illustrated in Fig. 21. The large decrease of the friction coefficient at the resonance peak can be seen, although for large rubbing velocity, when the rubbing energy dissipation is dominant, this increase becomes relatively small.

CONCLUSIONS

The formulation of the friction contact elements is developed which includes the effects of the prescribed relative motion on the friction stick-slip transitions and, therefore, on the contact interaction forces. For a first time, the formulation is made for the frequency domain analysis of coupled rubbing and vibrational motion, using the multiharmonic representation of the vibration displacements. The formulation is made fully analytically to express the multiharmonic contact interaction

forces and multiharmonic tangent stiffness matrix in an explicit analytical form allowing their calculation accurately and fast. The dependency of the friction coefficient on the energy dissipated during high-energy rubbing contacts and, hence, on the corresponding increase of the contact interface temperature is included in the formulation.

The efficiency of the developed friction elements is demonstrated on a set of test cases including simple models and a large-scale realistic blade. It is shown the significant effects of the gross rubbing motion on the vibration amplitudes and resonance peak frequencies.

REFERENCES

[1] Coulomb, C.A., (1785), Théorie des machines simples, en ayant égard au frottement de leurs parties et à la roideur des cordages. Tom. X of the Mémoires de Mathématique et de Physique Présentés à l'Académie Royale des Sciences, Par Divers Savans, pp. 161-332

[2] Armstrong-Hélouvry B., Dupont P. and De Wit C.C., (1994), A survey of models, analysis tools and compensations methods for the control of machines with friction. Automatica 30(7), pp. 1083– 1138

[3] Pennestrì E., Rossi V., Salvini P., Valentini, P., (2016), Review and comparison of dry friction force models, Nonlinear Dynamics, Volume 83, Issue 4, pp 1785–1801

[4] Marques F., Flores P.,·Claro P., Lankarani H., (2016), A survey and comparison of several friction force models for dynamic analysis of multibody mechanical systems, Nonlinear Dynamics, Vol.86, pp.1407–1443

[5] Iwan W. D., (1966), A Distributed-Element Model for Hysteresis and Its Steady-State Dynamic Response, ASME J. Appl. Mech., 33, pp. 893–900.

[6] Griffin J.H., (1980), Friction damping of resonant stresses in gas turbine engine airfoils, Trans. ASME: J. Eng. Gas Turbines and Power, Vol. 102, pp. 329-333

[7] Sanliturk K. Y. and Ewins D. J., (1996), Modelling two-dimensional friction contact and its application using harmonic balance method. J. of Sound and Vibration, Vol.193, pp.511-523

[8] Sextro W., (1996) The calculation of the forced response of shrouded blades with friction contacts and its experimental verification, Proc. of 2nd European Nonlinear Oscillation Conference, Prague, Sept. 9-13, 1996.

[9] Yang B. D. and Menq C. H., (1998), Characterization of 3D Contact Kinematics and Prediction of Resonant Response of Structures Having 3D Frictional Constraint, J. Sound and Vibration, 217(5), pp. 909–925

[10] Petrov E.P. and Ewins D.J., (2004), Generic friction models for time-domain vibration analysis of bladed discs, Trans. ASME: J. of Turbomachinery, Vol.126, January, pp.184-192

[11] Petrov E.P. and Ewins D.J., (2003), Analytical formulation of friction interface elements for analysis of nonlinear multi-harmonic vibrations of bladed discs, ASME J. of Turbomachinery, Vol.125, pp.364-371

[12] Zucca S., Firrone C.M., and Gola M.M., (2012). Numerical assessment of friction damping at turbine blade root joints by simultaneous calculation of the static and dynamic contact loads. Nonlinear Dynamics, 67(3): p. 1943-1955.

[13] Krack M., Salles L., and Thouverez F., (2017), Vibration prediction of bladed disks coupled by friction joints. Archives of Computational Methods in Engineering, 24(3), pp. 589–636.

[14] Jacquet-Richardet, G. et.al., (2013), Rotor to stator contacts in turbomachines. Review and application, Mechanical Systems and Signal Processing, Vol.40 (2), pp.401-420

[15] Childs D. and Bhattacharya A., (2007), Prediction of dry-friction whirl and whip between a rotor and a stator. J.Vib.Acoust. 129(3), 355–362)

[16] Petrov E.P., (2012), Mutliharmonic analysis of nonlinear whole engine dynamics with bladed disc-casing rubbing contacts, Proc. of ASME Turbo Expo 2012, June 11-15, 2012, Copenhagen, Denmark, GT2012-68474

[17] Batailly A., Legrand M., Millecamps A., Garcin F., (2012), Numerical-experimental comparison in the simulation of rotor/stator interaction through blade-tip/abradable coating contact, Trans. ASME: J. Eng. Gas Turbines and Power, Vol. 134(8), 082504

[18] Williams R. J., (2004), Parametric characterization of rub induced whirl instability using an instrumented rotordynamics test rig, Proc. Int. Conf. "Vibrations in rotating machinery, IMechE Conf. Trans., C623(012), pp. 651–660

[19] Williams R.J., (2011), Simulation of blade casing interaction phenomena in gas turbines resulting from heavy tip rubs using an implicit time marching method, Proc. of ASME Turbo Expo, GT2011-45495, Vancouver, Canada.

[20] Ouyang H., Nack W, Yuan Y. and Chen F., (2005), Numerical analysis of automotive disc brake squeal: a review, Int. J. Vehicle Noise and Vibration, Vol. 1, No. 3/4, pp.207-231

[21] Sawicki J., Montilla-Bravo A., (2003), Thermo-mechanical behavior of rotor with rubbing, Int. J. Rotating Mach. 9(1) 41–47.

[22] Bachschmid N., Pennacchi P. and Vania, A., (2007), Thermally induced vibrations due to rub in real rotors, J. Sound Vib, 299, pp. 683–719.

[23] Schwingshackl C.W., Petrov E.P. and Ewins, D.J., (2012), Measured and estimated friction interface parameters in a nonlinear dynamic analysis, Mechanical Systems and Signal Processing, Vol. 28, pp. 574-584

[24] Petrov E.P., (2011) A high-accuracy model reduction for analysis of nonlinear vibrations in structures with contact interfaces, Trans. ASME J. Eng. Gas Turbines and Power, Vol. 133(10), 102503

[25] Al Sayed B., Chatelet E., Baguet S. and Jacquet-Richardet G., (2011), Dissipated energy and boundary condition effects associated to dry friction on the dynamics of vibrating structures, Mechanism and Machine Theory, 46(4), pp. 479-491